

DEGS1-associated aberrant sphingolipid metabolism impairs nervous system function in humans

Gergely Karsai, Florian Kraft, Natja Haag, G. Christoph Korenke, Benjamin Hänisch, Alaa Othman, Saranya Suriyanarayanan, Regula Steiner, Cordula Knopp, Michael Mull, Markus Bergmann, J. Michael Schröder, Joachim Weis, Miriam Elbracht, Matthias Begemann, Thorsten Hornemann, Ingo Kurth

J Clin Invest. 2019. <https://doi.org/10.1172/JCI124159>.

Clinical Research and Public Health **In-Press Preview** **Genetics** **Metabolism**

Background. Sphingolipids are important components of cellular membranes and functionally associated with fundamental processes such as cell differentiation, neuronal signaling and myelin sheath formation. Defects in the synthesis or degradation of sphingolipids leads to various neurological pathologies, however, the entire spectrum of sphingolipid metabolism disorders remained elusive. **Methods.** A combined approach of genomics and lipidomics was applied to identify and characterize a human sphingolipid metabolism disorder. **Results.** By whole-exome sequencing in a patient with a multisystem neurological disorder of both the central and peripheral nervous system, we identified a homozygous p.(Ala280Val) variant in DEGS1, which catalyzes the last step in the ceramide synthesis pathway. The blood sphingolipid profile in the patient showed a significant increase in dihydro sphingolipid species which was further recapitulated in patient-derived fibroblasts, in CRISPR/Cas9-derived DEGS1 knockout cells, and by pharmacological inhibition of DEGS1. The enzymatic activity in patient fibroblasts was reduced by 80% compared to wild type cells which was in line with a reduced expression of mutant DEGS1 protein. Moreover, an atypical and potentially neurotoxic sphingosine isomer was identified in patient plasma and in cells expressing mutant DEGS1. **Conclusion.** We report DEGS1 dysfunction as cause for a novel sphingolipid disorder with hypomyelination and degeneration of both the central and peripheral nervous system. **Trial registration.** Not applicable. **Funding.** RESOLVE: Project number 305707; SNF: Project 31003A_153390/1; Rare Disease Initiative Zurich.

Find the latest version:

<https://jci.me/124159/pdf>



Aberrant DEGS1 sphingolipid metabolism impairs nervous system function in humans

Gergely Karsai^{1,2*}, Florian Kraft^{3*}, Natja Haag^{3*}, G Christoph Korenke⁴, Benjamin Hänisch³, Alaa Othman^{1,2}, Saranya Suriyanarayanan^{1,2}, Regula Steiner^{1,2}, Cordula Knopp³, Michael Mull⁵, Markus Bergmann⁶, J Michael Schröder⁷, Joachim Weis⁷, Miriam Elbracht³, Matthias Begemann³, Thorsten Hornemann^{1,2#} and Ingo Kurth^{3#}

*,# These authors contributed equally to this work.

¹ Center for Integrative Human Physiology, University of Zürich, 8091 Zürich, Switzerland.

² Institute for Clinical Chemistry, University Hospital, 8091 Zürich, Switzerland

³ Institute of Human Genetics, Medical Faculty, RWTH Aachen University, 52074 Aachen, Germany

⁴ Klinik für Neuropädiatrie und angeborene Stoffwechselerkrankungen, Universitätsklinik für Kinder- und Jugendmedizin, 26133 Oldenburg, Germany

⁵ Department of Diagnostic and Interventional Neuroradiology, Medical Faculty, RWTH Aachen University, 52074 Aachen, Germany

⁶ Institute for Neuropathology, Hospital Bremen-Mitte, 28205 Bremen, Germany

⁷ Institute of Neuropathology, Medical Faculty, RWTH Aachen University, 52074 Aachen, Germany

Correspondence should be addressed to I.K. (email: ikurth@ukaachen.de) or to T.H. (email: thorsten.hornemann@usz.ch)

Ingo Kurth

Institute of Human Genetics

Uniklinik RWTH Aachen

Pauwelsstr. 30

52074 Aachen

Germany

Phone +49-241-8080178

Thorsten Hornemann

Institute for Clinical Chemistry

University Hospital Zurich

Rämistrasse 100

8091 Zürich

Switzerland

Phone +41-44-255 47 19

Background. Sphingolipids are important components of cellular membranes and functionally associated with fundamental processes such as cell differentiation, neuronal signaling and myelin sheath formation. Defects in the synthesis or degradation of sphingolipids leads to various neurological pathologies, however, the entire spectrum of sphingolipid metabolism disorders remained elusive.

Methods. A combined approach of genomics and lipidomics was applied to identify and characterize a human sphingolipid metabolism disorder.

Results. By whole-exome sequencing in a patient with a multisystem neurological disorder of both the central and peripheral nervous system, we identified a homozygous p.(Ala280Val) variant in *DEGS1*, which catalyzes the last step in the ceramide synthesis pathway. The blood sphingolipid profile in the patient showed a significant increase in dihydro sphingolipid species which was further recapitulated in patient-derived fibroblasts, in CRISPR/Cas9-derived *DEGS1* knockout cells, and by pharmacological inhibition of *DEGS1*. The enzymatic activity in patient fibroblasts was reduced by 80% compared to wild type cells which was in line with a reduced expression of mutant *DEGS1* protein. Moreover, an atypical and potentially neurotoxic sphingosine isomer was identified in patient plasma and in cells expressing mutant *DEGS1*.

Conclusion. We report *DEGS1* dysfunction as cause for a novel sphingolipid disorder with hypomyelination and degeneration of both the central and peripheral nervous system.

Trial registration. Not applicable.

Funding. RESOLVE: Project number 305707; SNF: Project 31003A_153390/1; Rare Disease Initiative Zurich.

Keywords: neurodegeneration, leukodystrophy, peripheral neuropathy, sphingolipids,

DEGS1

Abbreviations: Cer = ceramides, dhCer = dihydroceramide, dhHexCer = dihydro-hexosylceramide, dhSM = dihydro-sphingomyelin, HexCer = hexosylceramide, HSAN = hereditary sensory and autonomic neuropathy, SA = sphinganine, SL = sphingolipids, SM = sphingomyelin, SO = sphingosine, SPT = serine-palmitoyltransferase, S1P = sphingosine-1-phosphate

Introduction

Sphingolipids (SL) are fundamental components of eukaryotic cell membranes where they play crucial roles in membrane architecture and signaling (1). They are major components of the myelin sheath and of fundamental importance for neural function (2). Whereas oligodendrocytes support and insulate neurons of the central nervous system (CNS), equivalent function is provided by Schwann cells in the peripheral nervous system (PNS). Besides a role in myelin sheath formation and maintenance, signaling SLs such as sphingosine-1-phosphate (S1P) and ceramide-1-phosphate are bioactive lipid hormones that regulate a variety of physiological functions. Ceramides are central components of the SL metabolism as they form the building blocks for complex SLs like sphingomyelin and glycosylceramides. They also represent the crossroad for the degradation and salvage pathways (3). Ceramide biosynthesis starts at the endoplasmic reticulum (ER) with the conjugation of L-serine and palmitoyl-CoA, the rate-limiting step catalyzed by serine-palmitoyltransferase (SPT). The immediate product 3-keto-sphinganine is reduced to sphinganine (SA) which is then N-acylated to dihydroceramide (dhCer) by one of six ceramide synthase isoforms (CerS1-6) (4). In the final step, dhCer is converted to ceramide (Cer) by the insertion of a Δ 4,5-trans (Δ 4E) double bond into the sphinganine backbone. This final conversion is catalyzed by the Δ 4-dihydroceramide desaturase (DEGS1) (5). On the catabolic side, ceramides are deacylated by ceramidases to form sphingosine (SO) which can be either recycled back to ceramides (salvage pathway) or phosphorylated by sphingosine kinases (SK1/SK2) to form sphingosine-1-phosphate (S1P). S1P is a potent lipid hormone that binds to specific S1P receptors (SP1R1-6), which control a multitude of cellular responses (6). S1P can either be converted back to SO through action of S1P phosphatases (S1PPase), or terminally degraded by the S1P lyase (SGPL1) to hexadecenal and ethanolamine phosphate (7). For complex SL formation,

ceramides are transported from the ER to the Golgi and are converted into phosphosphingolipids (e.g. sphingomyelin) or glycosphingolipids (GalCer, GluCer). Subsequently, they are metabolized to highly complex glycosphingolipids such as gangliosides (8).

The degradation of complex SLs requires dedicated catabolic enzymes, such as glycohydrolases and sphingomyelinases that reside in the plasma membrane, ER, Golgi apparatus and lysosomes (9, 10).

Defects in these catabolic enzymes cause sphingolipidoses such as M. Fabry, M. Gaucher, M. Farbers, M. Niemann-Pick and M. Tay-Sachs (11). Vice versa, defects in the synthesis pathway are also associated with disease. Mutations in SPT (*SPTLC1* and *SPTLC2*) lead to the formation of aberrant and neurotoxic 1-deoxysphingolipids which result in hereditary sensory and autonomic neuropathy type I (OMIM #162400, #613640) (12). Genetic variants in ceramide synthase 1 and 2 (*CERS1/2*) are associated with progressive myoclonic epilepsy, generalized tonic-clonic seizures, tremor, dysarthria, ataxia and developmental delay (OMIM #616230) (13-15). Mutations in the GM3 synthase gene (*ST3GAL5*) lead to refractory epilepsy, psychomotor delay, blindness, and deafness (OMIM #609056) (16, 17) and GM2/GD2 synthase mutations (*B4GALNT1*) lead to GM3 accumulation and a complex form of hereditary spastic paraparesis with cognitive impairment and seizures (OMIM #609195) (18). Recently, mutations in *SGPL1* were associated with a broad spectrum of disease phenotypes including recessive steroid-resistant nephrotic syndrome (SRNS), ichthyosis, adrenal insufficiency, immunodeficiency, and brain defects (OMIM #617575) (19-21), but also with axonal peripheral neuropathy without renal or adrenal deficiencies (22).

Here, we identify *DEGS1* dysfunction as cause for a novel sphingolipid disorder with leukodystrophy and hypomyelination of the peripheral nervous system.

Results

Clinical description and genetic analysis

The 22-year old male patient was first-born from healthy consanguineous Turkish parents and showed a progressive mixed pyramidal and extrapyramidal movement disorder as well as a progressive cerebellar atrophy. At the age of 6 months a motor developmental delay was observed and progressive spasticity became obvious in the further clinical course (**Figure 1A-D, Supplemental Video**). Consecutive brain MRI revealed a general hypomyelination, a thinning of the brainstem and occipital white matter, severely reduced volume of both thalami, progressive cerebellar and supra- and infratentorial atrophy and a thin corpus callosum, most pronounced in the dorsal part (**Figure 1E-J**). In the clinical course, he developed a pathological EEG with epilepsy and grand mal seizures, which were successfully treated by a combination of valproate and carbamazepine. He showed a progressive neurological dysfunction, microcephaly, dystrophy, a progressive scoliosis, neurogenic bladder, and gastroesophageal reflux. Since age of 18 years, feeding required a percutaneous endoscopic gastrostomy. Progressive spasticity resulted in flexion contractures of the extremities, a positive Babinski sign, and increased muscle tone. At the age of 19 years, an intrathecal baclofen pump therapy was initiated. Detailed clinical findings are summarized in **Table 1**. A muscle and N. suralis biopsy was performed at the age of 2 years. Archived electron micrographs (**Figure 1K-N**) from the sural nerve biopsy showed several nerve fibers with disproportionately thin myelin sheaths, moderate myelin folding, widening of the endoplasmic reticulum of Schwann cells and several autophagic vacuoles in the cytoplasm of Schwann cells. The muscle biopsy revealed neurogenic muscular atrophy according to the records that could be retrieved, however, no muscle specimens were available for review.

Electroneurography at both arms and legs showed significantly slowed nerve conduction velocities with only a slight reduction of the amplitudes in line with a predominant demyelinating neuropathy. Metabolic screening for lysosomal storage disorders did not show pathological findings. Genetic workup revealed a normal male karyotype (46, XY) and array-CGH was unsuspicious (not shown).

Using whole-exome sequencing in the index patient, his two unaffected siblings as well as both parents revealed a suspicious homozygous missense variant in the index patient in *DEGS1* (NM_003676.3) (**Figure 1O-Q** and **Supplemental Table 1**). Both parents and the siblings were heterozygous carriers of this *DEGS1* variant (**Figure 1O**). The variant changes the codon 280 from Alanine to Valine (p.Ala280Val) (**Figure 1P**), affecting a highly conserved nucleotide (c.839C>T) and amino acid (**Figure 1Q**). The altered residue is located in the fatty acid desaturase / sphingolipid delta 4-desaturase domain. The variant was not present in public databases (dbSNP, 1000genomes, ESP server, ExAC and gnomAD) and was predicted to be deleterious by several bioinformatics pathogenicity prediction tools (CADD_phred (35), SIFT (0), Polyphen2_HDIV (0,99), MutationTaster prediction (D)).

Splicing, subcellular localization and expression of mutant *DEGS1*

Besides a codon change from alanine to valine (p.Ala280Val), the software tools NNSplice and GeneSplicer predicted a possible splicing effect for the c.839C>T variant in *DEGS1*. To address an influence on splicing, we used third-generation long-read nanopore sequencing of cDNA from patient fibroblasts and did not observe aberrant transcripts compared to cDNA from control fibroblasts and reference transcripts (**Figure 2A**).

To investigate whether the p.Ala280Val variant (mut *DEGS1*) affects subcellular localization, we overexpressed EGFP-tagged wildtype (wt) and mut *DEGS1* in HeLa cells. Cells were co-

stained with markers for endoplasmic reticulum (ER) and mitochondria (**Figure 2B-E**). Both wt and mut DEGS1 co-localized with the ER marker protein disulfide isomerase (PDI) (**Figure 2B, C**) and showed only little co-localization with the mitochondrial marker Tim23 (**Figure 2D, E**). Notably, DEGS1 expression levels were reduced in patient fibroblasts compared to controls as determined by western blot (**Figure 2F, G**). To further analyze the DEGS1 mutation, *DEGS1* and the homologous *DEGS2* were knocked out in HAP1 cells by CRISPR/Cas9 technology (*DEGS1*^{-/-}, *DEGS2*^{-/-}). Similarly to the expression in fibroblasts, overexpression of mut DEGS1-EGFP in HAP1 cells resulted in a lower protein amount compared to wt DEGS1-EGFP (**Figure 2H, I**). FACS measurements of HAP1 WT cells transfected with wt or mut DEGS1 fused to EGFP in addition showed a lower number of GFP positive cells (**Supplementary Figure 1**). Moreover, inhibiting protein translation with cycloheximide (CHX) in HAP1 WT cells overexpressing either wt or mut DEGS1-EGFP indicated a reduced half-life of the mutant. Conversely, treating cells with the proteasome inhibitor MG-132 stabilized both wt and mut DEGS1 protein (**Figure 2H, J**). This implies that the mutation p.Ala280Val affects overall DEGS1 protein stability.

Sphingolipid analysis

We performed an untargeted lipidomics analysis from plasma of the index patient, his parents and six unrelated controls. Total SL plasma levels were comparable between the individuals, however, the patient plasma revealed a striking overrepresentation of dihydrosphingolipid (dhSL) species (dhSM, dhCer and dhHexCer) compared to parents and controls (**Figure 3A**). The relative proportion of dhSLs in patient plasma was about 40 %, while it was about 10 % in controls and parents. This disproportion was confirmed in patient-derived skin fibroblasts. SL *de novo synthesis* was measured by culturing the fibroblasts in the presence of stable isotope labeled d4-serine which is incorporated in *de novo* formed sphingoid bases. Like in plasma,

we observed a significantly increased formation of dhSL species in patient fibroblasts compared to control cells (**Figure 3B**). To confirm that this shift is directly caused by DEGS1 dysfunction, we used the *DEGS1* and *DEGS2*-deficient HAP1 lines. In *DEGS1*^{-/-} cells, about 90 % of the de novo formed SLs were present in the saturated dihydro form, whereas *DEGS2*^{-/-} cells showed no changes in the profile. Interestingly, the relative levels of dhSLs were lower in patient derived fibroblasts (40%) compared to *DEGS1*^{-/-} cells (90%), suggesting that the *DEGS1* p.A280V mutant may have some residual activity. We therefore analyzed *DEGS1* activity in patient fibroblasts by measuring the conversion of stable isotope labeled d7-sphinganine (d7SA) to d7-sphingosine (d7SO) (**Figure 3C**). In patient fibroblasts a slow conversion between the two forms was observed, indicating that the p.A280V mutant still has some activity. Compared to control fibroblasts, the rate was about five-fold lower indicating a residual activity of about 20%. This remaining activity was completely suppressed in presence of the *DEGS1* inhibitor Fenretinide (4-HPR) (**Figure 3C**).

DEGS1 deficiency results in the formation of a novel sphingoid base

Surprisingly, when analyzing the sphingoid base profile in hydrolyzed plasma samples we observed a second peak which was isomeric to SO. The peak was detected in the patient plasma but not in plasma of the parents or unrelated controls (**Figure 3D**). The metabolite had the same exact mass as SO, but a 30 second earlier retention time. To prove that this peak is a bona-fide sphingoid base, we performed an isotope-labeling assay, supplementing d4-serine to HAP1 WT and *DEGS1*^{-/-} cells. This resulted in the formation of canonical SO+3 in HAP1 WT cells and in the +3 labelled isomeric peak in *DEGS1*^{-/-} cells (**Figure 4A**). The same labelling pattern was observed in control fibroblasts when *DEGS1* activity was inhibited with 4-HPR (**Figure 4A**) confirming that this novel metabolite is directly associated with a reduced *DEGS1*

activity. Furthermore, the metabolite was not formed when SPT activity was inhibited with myriocin indicating that the formation is downstream of SPT (**Supplemental Figure 2A**). To gain further insight into the metabolic origin of this atypical sphingoid base, we supplemented DEGS1^{-/-} cells either with isotope labelled d7SA or d7SO. In d7SA supplemented cells the isomeric metabolite was formed quantitatively and isotope labelled (+7) whereas d7SO was not converted and reappeared in the cells as SO+7 with the expected retention time for the canonical SO. This indicated that the novel metabolite is indeed a downstream product of SA and not a direct product of SPT (**Figure 4B**). A structural analysis using chemical derivatization with dimethyl disulfide followed by collision induced HCD fragmentation (23), revealed a specific fragment (m/z 110.10156) reflecting an isotope labelled four carbon tail fragment of SO+7 (**Figure 4C**). This suggests, that the double bond position of the isomeric sphingosine metabolite is in Δ14 position and distinct to the Δ4 position of canonical SO. This result was further confirmed by supplementing DEGS1^{-/-} cells with d4(C₁₁-C₁₂) labelled palmitate. When incorporated into the sphingoid base, the d4(C₁₁-C₁₂) palmitate is converted to SA+4 with four deuterium labels at C₁₃ - C₁₄ position (**Supplemental Figure 2C**). Introducing a Δ4 double bond will not affect the label whereas a Δ14 double bond results in the loss of one deuterium. As expected, canonical SO (Δ4) was found to be exclusively +4 labelled (**Supplemental Figure 2C**) whereas the isomeric pre-peak contained the +3 label, which further supports a Δ14 position of the double bond.

Supplementation of a sphingolipid rich diet as a therapeutic intervention

Correcting the altered dhSL/SL ratio in the patient was considered as potential therapeutic approach for the DEGS1-disorder. SLs are abundantly present in meat, milk and egg products (24), whereas plants and yeast usually have phytosphingolipids (phytoSL) that bear a C4

hydroxyl group instead of the $\Delta 4$ double bond. An increased dietary SL consumption from animal products might therefore increase the levels of unsaturated SL species, thereby lowering the dhSL/SL ratio in the patient. Therefore, we tested whether the sphingolipid profile of the patient may be positively influenced by dietary intervention. The pilot study started with a two week “washout phase” providing a primarily plant based vegetarian diet. Subsequently, the patient was fed with an animal-based diet (milk, eggs and meat) for another two weeks. Plasma samples were taken before and after the “washout phase” and at the end of the supplementation period. The patient reported no adverse side effects except for improved bowel movement during the vegetarian diet. However, the supplementation only had a minor effect on the plasma sphingoid base profile (**Supplemental Figure 2D**). We observed a small increase in phytoSL levels after the vegetarian phase and in total SL levels at the end of the supplementation period, but unfortunately no significant change in the dhSL/SL ratio.

Discussion

Here we report on a 22-year old male patient with a multisystem disease with hypomyelination and degeneration of both the central and the peripheral nervous system. Leading symptoms were early-onset developmental delay, movement disorder, progressive spasticity and epilepsy. Similar disease hallmarks may be seen in mitochondriopathies, neuronal ceroid lipofuscinosis, lysosomal storage disorders, or leukodystrophies, however, none of these diagnoses could be confirmed in the index patient. Instead, whole-exome sequencing identified a single nucleotide exchange in *DEGS1* (c.893C>T) leading to an amino acid exchange (p.Ala280Val) in a highly conserved region of the respective protein. *DEGS1* is a central enzyme in the sphingolipid de novo synthesis pathway (**Supplemental Figure 3**) and has yet not been associated with a human monogenic disease. The enzyme catalyzes the final conversion of dhCer into Cer by introducing a Δ4,5 trans double bond into the sphingoid base backbone (25). *DEGS1* is a transmembrane protein residing in the endoplasmic reticulum (ER) and contains three conserved histidine-based motifs characteristic for membrane lipid desaturases and membrane hydrocarbon hydroxylases (5, 26, 27). Both, pharmacological and genetic ablation of *DEGS1* leads to an accumulation of its substrate dhCer (28). Both, dhCer and Cer can be metabolized to complex sphingolipids although the majority of SLs contains a SO(Δ4E) whereas SA based dhSL species are minor. However, lipidomics analysis of the patient plasma revealed significantly elevated dhSL levels indicating that the desaturase activity in the p.Ala280Val variant is reduced. Elevated levels of dhSL species were also seen in patient-derived fibroblasts and kinetic studies revealed a residual activity of about 20 % for mutant compared to wildtype protein. Mutant *DEGS1* showed a reduced expression in skin-derived fibroblasts and expression levels in transfected HAP1 cells were reproducibly lower than for the wildtype. Western blot quantification showed an about 80 % reduced expression of the

mutant protein in patient fibroblasts, which could explain the 20 % residual activity of DEGS1 in these cells.

DEGS2, a homolog isoform of DEGS1 (29) was reported to act as a bifunctional enzyme with either a C4-monoxygenase activity adding a hydroxyl group to the C4 position forming phytosphingolipids, or a delta(4)-desaturase activity similar to DEGS1. However, DEGS2 was not able to compensate for the enzymatic loss in DEGS1-deficient HAP1 cells, indicating mutually exclusive roles for both homologs.

In mice, homozygous deletion of *Degs1* (*Degs1*^{-/-} mice) is lethal, however with incomplete penetrance. Surviving pups were small and revealed a complex phenotype including scaly skin and sparse hair, tremor, and metabolic abnormalities (28). *Degs1*^{-/-} mice had less ceramide levels and dramatically more dhCer in blood and tissues compared to wildtype littermates. Heterozygous *Degs1*^{+/−} animals showed improved insulin sensitivity on high-fat diet and were resistant to dexamethasone induced insulin resistance (28). This and subsequent observations indicated that a moderate increase in the dhCer/Cer ratio is linked to an improved glucose metabolism and metabolic control, although the underlying physiological mechanisms are not yet fully understood (30, 31). Notably, we did not observe a significant difference in the dhSL levels between the heterozygous parents and unrelated controls.

An increased dhSL/SL ratio results in higher rigidity of the plasma membrane (32), which likely affects many biological processes relying on appropriate membrane dynamics for active transport, diffusion, vesicle formation and signaling. It is tempting to speculate that alterations in the ER structure, as observed in the EM of the sural nerve of the patient may reflect impaired membrane properties. However, defects in DEGS1 not only influences the dhCer/Cer ratio but also the profile of complex sphingolipids like (dh)SM and (dh)HexCer which are formed downstream of dhCer. Sphingomyelin (SM) is an abundant component of

glia and myelin and the distinct biophysical properties of dhSM might significantly affect the physiology of glia cells and the structure of the myelin sheath. Indeed, myelin has a special membrane structure with a unique molecular composition and architecture. The most striking features are high levels of plasmalogens and the enrichment of specific glycosphingolipids. Several structural aspects distinguish glycosphingolipids in myelin from glycosphingolipids found in the plasma membrane of most other cell types. In particular, head groups are primarily based on galactose instead of glucose, and a relatively high proportion of hydroxylated fatty acids and the incorporation of very-long-chain fatty acids with chain lengths up to 26 carbons are characteristic. Even minor perturbations in this molecular composition lead to myelination defects (33), which likely explains the hypomyelination in our patient.

In addition to the increased dhSL levels, we also identified a novel, atypical sphingolipid metabolite which seems to be specifically formed under conditions of a reduced DEGS1 activity. This metabolite was isomeric to SO but eluted with a slightly shifted retention time compared to canonical SO. The novel metabolite was prominently present in plasma of the index patient, in DEGS1^{-/-} HAP1 cells as well as in fibroblasts treated with the DEGS1 inhibitor 4-HPR. It was isotope labeled with d4-serine proving it as a bona-fide sphingolipid and downstream product of SPT and can be directly formed from d7SA but not from d7SO. Further structural elucidations revealed that this isomeric SO contains a double bond at Δ14 instead of Δ4 position. Sphingoid bases with a Δ14 double bond were reported earlier. First for sphingadienine, a polyunsaturated downstream metabolite of SO, and recently also for 1-deoxySO, an aberrant sphingoid base formed by mutant SPT enzymes in the context of the sensory and autonomic neuropathy type 1 (23). In both cases, the Δ14 double bond was found to be in cis (Z) conformation which likewise suggests a Δ14 double bond of the isomeric SO in

cis (Z) conformation (SO(14Z)). The double bond is likely formed by a not yet identified Δ 14-15Z desaturase in an alternative reaction to *DEGS1*. The toxicity and pathophysiological relevance of this atypical SO isomer is not clear, but may be a crucial part of the pathomechanism. As a cis (Z) conformation introduces a kink into the structure of the sphingoid base, the lateral assembly with other membrane lipids will be different than for canonical SO that contains a straight (Δ 4E) double bond. Both, the elevation in dhSL species and the SO(14Z) isomer might be relevant for the observed hypomyelination phenotype.

In a pilot experiment we tested whether the serum dhSL/SL ratio could be influenced by a diet rich in canonical SLs. However, we were not able to modulate the dhSL/SL ratio in the patient, but this two-week test phase may be too short or the dietary intervention to inefficient to observe a significant metabolic effect.

In summary, we identified *DEGS1* as novel disease-causing gene implicated in a heritable multisystem disorder with hypomyelination and degeneration of both the central and the peripheral nervous system. The mutation affects the sphingolipid de novo synthesis leading to an altered dhSL/SL ratio and results in the formation of an aberrant and potentially neurotoxic SO isomer.

Methods

Neuropathology

Resin embedding of the glutaraldehyde-fixed sural nerve biopsy tissue and subsequent electron microscopy had been performed using standard procedures (34).

Whole-exome sequencing

Whole-exome Sequencing was performed with the DNA from peripheral blood of five family members including the index case, the two unaffected siblings and both parents. Enrichment was done with an Illumina Enrichment Kit (Nextera Rapid Capture Exome v1.2) and the respective libraries were sequenced on a NextSeq500 sequencer (Illumina, San Diego, USA). Alignment and variant calling was performed with SeqMule (v1.2) (35), (FastQC (version: 0.11.2), BWA-MEM (version: 0.7.8-r455), SAMtools (rmdup; version: 0.1.19-44428cd), SAMtools (filter; version: 0.1.19-44428cd), SAMtools (index; version: 0.1.19-44428cd, and GATKLite (realign; version: 2.3-9-gcdccbb). Genome version hg19 was used for the alignment. Three variant callers were applied for variant detection (GATKLite UnifiedGenotyper (variant; version: 2.3-9-gcdccbb), SAMtools (mpileup; version: 0.1.19-44428cd), FreeBayes (version: 0.9.14-14-gb00b735)). Variants called by at least two programs were considered for further analysis. The resulting variant files were combined (GATK, v3.6, CombineVariants) and processed with KGGSeq (v1.0, 14/Apr./2017) (36). Variants with a Minor Allele Frequency in public databases (i.e. ExAC, GnomAD, ESP, 1kG) above 0.75% were excluded. Average coverage in the target region was between 90-142x with 88-92% above 20x coverage, respectively. Mutations were confirmed by sanger sequencing with BigDye

Terminator 3.1 cycle sequencing kit and Genetic Analyzer 3500 (ThermoFisher Scientific, Darmstadt, Germany).

Cells and cell culture

DEGS1 and DEGS2 knock out cells (DEGS1^{-/-} HAP1, DEGS2^{-/-} HAP1) were generated by a commercial service (Horizon Discovery, Waterbeach, United Kingdom). The introduction of a frame-shift mutation was confirmed by sequencing. HAP1 WT cells were provided as controls. HAP1 cells were cultured in Iscove's Modified Dulbecco's Medium (IMDM, ThermoFisher Scientific, Darmstadt, Germany) supplemented with 10 % fetal calf serum, 4mM L-Glutamine and 1 % penicillin/streptomycin at 37°C in a 5 % CO₂ atmosphere. Patient fibroblasts were derived from a tissue biopsy in the index patient. HeLa (ATCC CCL-2) and BJ-5ta (ATCC CCL-2) cells were cultured in Dulbecco's modified Eagle's medium (DMEM, ThermoFisher Scientific, Darmstadt, Germany) supplemented with 10 % fetal calf serum and 1 % penicillin/streptomycin at 37 °C in a 5 % CO₂ atmosphere. Transfection of HeLa cells (ATCC CCL-2) and HAP1 cells was done using Polyjet or GenJet in vitro transfection reagent (SigmaGen, Rockville, Maryland, USA) according to manufacturer's protocol.

Immunohistochemistry

Transfected cells were fixed after 24 h with 4% paraformaldehyde in PBS. After blocking and permeabilization with 2 % bovine serum albumine, 10 % normal goat serum and 0.25 % TritonX-100 in PBS for 60 min at room temperature, cells were incubated with primary antibodies in blocking solution for 60 min at room temperature, washed 3 times in PBS and

incubated with Alexa Fluor-568 or -647 secondary antibodies (1:1000; Molecular Probes). DAPI (4',6-diamidino-2-phenylindole, 1:1000; Invitrogen) was used for nucleic acid staining. Images were taken with a Zeiss Observer Z.1 microscope equipped with an Apotome2 and HXP 120 lamp. The following primary antibodies were used: mouse-anti-PDI (Enzo, ADI-SPA-891, 1:200), mouse-anti-Tim23 (BD 611222, 1:200).

Cycloheximide chase

Transfected HAP1 cells were treated with cycloheximide (25 µg/ml) with or without 10 µM MG-132 for the indicated time-period. Cells were harvested with cell scrapers in ice-cold PBS and pelleted by centrifugation at 500 g for 5 min.

Western blot

Protein isolation and Western Blot were carried out as described elsewhere (37). The primary antibodies used for immunodetection were DEGS1 (Abcam, ab167169, 1: 5000), GFP (Millipore, MAB3580, 1:1000) and α -tubulin (Abcam, ab15246, 1: 2000). As secondary antibodies, horseradish peroxidase-conjugated anti-rabbit (Santa Cruz, sc-2370, 1: 10000) and anti-mouse IgGs (Santa Cruz, sc-2005, 1: 10000) were used. Detection was done using Clarity Western ECL Substrate (Bio-Rad, Munich, Germany) and FujiFilm LAS 3000 system (FujiFilm, Düsseldorf, Germany). PageRuler or PageRuler Plus Prestained Protein Ladder (ThermoFisher Scientific, Darmstadt, Germany) was used for protein weight estimation.

Cloning

Human DEGS1 (NM_003676.3) was amplified from a commercially available cDNA library, using the following primers (Forward: caccatggggagccgcgtctcgccggaaagacttc, Reverse:

ctccagcaccatctccctttgggt). The amplicon for DEGS1 lacking the stop codon was subcloned into pEGFP vectors (Clontech, Saint-Germain-en-Laye, France). The mutation p.Ala280Val was introduced by targeted mutagenesis. pEF1 α -DEGS1-EGFP and DEGS1-EGFP (c.893C>T) were generated by cutting pEGFP-DEGS1 with AflIII and EcoRI and blunted by Klenow fragment. pEF1 α -Tet3g was digested with EcoRI and HindIII and ends were filled by Klenow fragment followed by dephosphorylation with FastAP. The resulting fragments were ligated with T4 ligase. All inserts were sequence verified using Sanger sequencing.

FACS

Transfected cells were trypsinized, pelleted and resuspended in PBS containing 250 ng/ml 7-AAD (BioLegend) for live/dead cell discrimination. Measurements were carried out on a Canto II flow cytometer (Becton Dickinson, New Jersey, USA). For lipidomics, cell pellets were resuspended in PBS containing 250 ng/ml 7-AAD and 20 % FCS. Sorting was carried out on an Aria II cell sorter (Becton Dickinson, New Jersey, USA) and 300,000 GFP positive and negative cells were collected per sample.

Lipidomics

Lipid extraction was performed as described previously (38) with some modifications. 20 μ l plasma sample or 0.5-5 million cells were suspended in 20 μ l PBS, 1 ml of a mixture of methanol: MTBE: chloroform (MMC) 4:3:3 (v/v/v) was added. The MMC mix was fortified with 100 pmoles/ml of the internal standards: d7-sphinganine (d18:0), d7-sphingosine (d18:1), dihydroceramide (d18:0:12:0), ceramide (d18:1/12:0), glucosylceramide (d18:1/8:0), sphingomyelin (18:1/12:0) and 50 pmoles/ml d7-sphingosine-1-phosphate. After brief vortexing, the samples were continuously mixed in a Thermomixer (Eppendorf) at 37 °C (1400

rpm, 20 min). Protein precipitation was obtained after centrifugation for 5 min, 16.000 g, 25 °C. The single-phase supernatant was collected, dried under N2 and stored at –20 °C until analysis. Before analysis, the dried lipids were dissolved in 100µl MeOH.

Liquid chromatography was done according to (39) with some modifications. The lipids were separated using a C30 Accucore LC column (Thermo Scientific, 150 mm * 2.1 mm * 2.6 µm) using the following mobile phases; A) Acetonitrile:Water (2:8) with 10 mM ammonium acetate and 0.1 % formic acid, B) Isopropanol: Acetonitrile (9:1) with 10 mM ammonium acetate and 0.1 % formic acid and C) methanol at a flow rate of 0.3 ml/min.

The following gradient was applied; 0.0-1.5 min (isocratic 70 %A, 20 %B and 10 %C), 2. 1.5-18.5 min (ramp 20-100 % B), 3.18.5-25.5 min (isocratic 100 %B) 4. 25.5-30.5 minutes (isocratic 70 %A, 20 %B and 10 %C).

The liquid chromatography was coupled to a hybrid quadrupole-orbitrap mass spectrometer Q-Exactive (Thermo Scientific, Reinach, BL, Switzerland), samples were analyzed in positive mode using a heated electrospray ionization (HESI) interface. The following parameters were used: spray voltage 3.5 kV, vaporizer temperature of 300 °C, sheath gas pressure 20 AU, aux gas 8 AU and capillary temperature of 320 °C. The detector was set to an MS2 method using a data dependent acquisition with top10 approach with stepped collision energy between 25 and 30. A 140 000 resolution was used for the full spectrum and a 17500 for MS². A dynamic exclusion filter was applied which will excludes fragmentation of the same ions for 20 sec. Identification criteria were 1) resolution with an accuracy of 5 ppm from the predicted mass at a resolving power of 140000 at 200 m/z. 2) Isotopic pattern fitting to expected isotopic distribution. 3) matching retention time on synthetic standards if available. and 4) the specific fragmentation patterns. Quantification was done using single point calibration. Pool samples in four concentration were used as quality controls.

Metabolic labelling and sphingoid base profiling

250.000 cells were seeded in 2 ml fresh medium in six-well plates (BD Falcon) and cultured for 2 days reaching ~70–80% confluence. The medium was exchanged for L-serine- and L-alanine-free DMEM (Genaxxon Bioscience, Ulm, Germany), containing 10% FBS(Fisher Scientific; FSA15-043) and 1 % penicillin / streptomycin (100 units per mL / 0.1 mg/mL, Sigma). Two hours after medium exchange, isotope-labelled d3-N15-L-serine (1 mM) and (2,3,3,3)-d4-L-alanine (2 mM) was added (Cambridge Isotope Laboratories, Tewksbury, Massachusetts, United States). In certain cases, Myriocin (Focus Biomolecules, Plymouth Meeting, PA USA) or d7SA/d7SO (Avanti Polar Lipids, Alabaster, CA, USA) was also added to the cells. Palmitate labelling was performed in DMEM (Sigma) with 10 % FBS (Fisher Scientific; FSA15-043) and 1 % penicillin / streptomycin supplemented with 25 μ M d4 Palmitic acid (Cambridge Isotope Laboratories, Tewksbury, Massachusetts, United States). After 24 h, cells were harvested in 1 ml cold phosphate-buffered saline (PBS), counted (Beckman Coulter Z2), pelleted at 600 RCF at 4°C and stored at –20°C until further processing. During the SPT reaction, one deuterium from serine is exchanged by a hydrogen, which results in newly formed sphingoid bases with a d3 isotope label. In some cases, the quantification of isotope labelled sphingoid bases was simplified by hydrolyzing the extracted lipids prior MS analysis (40). During hydrolysis, the conjugated N-acyl chains and attached head groups are removed and the SL backbones released as free sphingoid bases. Dihydro-SL species are converted to free SA and unsaturated species to free SO.

Dimethyl disulfide adduct analysis by LC-MS

Dimethyl disulfide (DMDS, 100 μ l) and 20 μ l of I2 (in diethylether, 60 mg/ml) were added to whole cell extracts or 15 nmol SPH m18:1(4E)(3OH) standard. Samples were agitated for 16 h in an Eppendorf Thermo shaker at 1,400 rpm and 47°C. The reaction was quenched with 100 μ l of 5% aqueous Na2S2O3, extracted with 200 μ l of hexane, and dried under N2. Samples were dissolved in 50 μ l Methanol: water (1:1) for further analysis according to the method of Dunkelblum, Tan, and Silk (9) with some modifications. The DMDS adducts were separated using a C30 Accucore LC column (Thermo Scientific, 150 mm * 2.1 mm * 2.6 μ m) and the following mobile phases; A) MeOH:H2O (1:1) with 10 mM ammonium formate and 0.1 % formic acid, B) Methanol at a flow rate of 0.3ml/min using a TLX Transcend pump (Thermo Scientific, Reinach, BL, Switzerland). The following gradient was applied; 1) 0.0-1.0 min (isocratic 10 %B), 2) 1.0-26.0 min (ramp 10-100 % B), 3) 26.0-32.0 min (isocratic 100 % B) 4) 32.0-33.0 minutes (ramp 100-10 % B) and 5) 33.0-35.0 (isocratic 10 % B).

The liquid chromatography was coupled to a hybrid quadrupole-orbitrap mass spectrometer Q-Exactive (Thermo Scientific, Reinach, BL, Switzerland), samples were analyzed in positive mode using a heated electrospray ionization (HESI) interface. The following parameters were used: spray voltage 3.5 kV, vaporizer temperature of 100 °C, sheath gas pressure 40 AU, aux gas 10 AU and capillary temperature of 300 °C. The mass spectrometer was operated in two alternating scan modes 1) full scan mode at 140000 resolution, 3e6 AGC target and a scan range form 150-900 m/z. and 2) parallel reaction monitoring mode (PRM) at 70000 resolution, 2e5 AGC target, 200 ms maximum injection time and 1.5 m/z isolation window. The normalized collision energy was set to 35, 50 and 70. The inclusion list for the PRM included both the non-labeled sphingosine DMDS adduct (m/z 394.28080) and the d7 labeled sphingosine DMDS adduct (m/z 401.32473).

Statistics

Results are mean \pm SD or mean - SD from at least 3 independent experiments using GraphPad Prism 8. Statistical analysis was conducted using 2-way ANOVA, using Tukey's correction for multiple comparisons. P value of less than 0.05 was considered statistically significant. *P < 0.05; **P < 0.01; ***P < 0.001.

Study approval

Written informed consent was obtained from the study participants after approval from the Institutional Review Boards at the participating institutions (Uniklinik RWTH Aachen: EK302-16). Consent was obtained according to the Declaration of Helsinki and consent was given for the publication of patient photographs and video.

Author contributions

I.K., G.C.K. and T.H. designed the study. G.C.K., C.K., M.M. and M.E. assessed the phenotype of the patient. M.B., J.M.S. and J.W. did the neuropathological analysis. Exome sequencing and evaluation was done by M.Begemann, F.K., I.K.. Lipidomics studies were performed and evaluated by G.K., A.O., S.S., R.S. and T.H.. Cell biological experiments were done by F.K., N.H. and B.H..

Declaration of interests: The authors have declared that no conflict of interest exists.

Acknowledgements

We are grateful to the family participating in the study. The authors declare no conflict of interest. We thank Sebastian Gießelmann for excellent technical support. We thank Dr. Steuernagel, Klinikum Oldenburg, for initial fibroblast cultures. This work was supported by grants of the German Charcot–Marie-Tooth Disease Network (CMT-Net; 01GM1511D) to J.W.. Funding of the 7th Framework Program of the European Commission ("RESOLVE", Project number 305707); the Swiss National Foundation SNF (Project 31003A_153390/1); the Hurka Foundation; the Novartis Foundation and the Rare Disease Initiative Zurich ("radiz", Clinical Research Priority Program for Rare Diseases, University of Zurich) to T.H..

References

1. Hannun YA, and Obeid LM. Sphingolipids and their metabolism in physiology and disease. *Nat Rev Mol Cell Biol.* 2018;19(3):175-91.
2. Hannun YA, and Obeid LM. Principles of bioactive lipid signalling: lessons from sphingolipids. *Nat Rev Mol Cell Biol.* 2008;9(2):139-50.
3. Bikman BT, and Summers SA. Ceramides as modulators of cellular and whole-body metabolism. *J Clin Invest.* 2011;121(11):4222-30.
4. Levy M, and Futerman AH. Mammalian ceramide synthases. *IUBMB Life.* 2010;62(5):347-56.
5. Ternes P, Franke S, Zahringer U, Sperling P, and Heinz E. Identification and characterization of a sphingolipid delta 4-desaturase family. *J Biol Chem.* 2002;277(28):25512-8.
6. Ogretmen B. Sphingolipid metabolism in cancer signalling and therapy. *Nat Rev Cancer.* 2018;18(1):33-50.
7. Merrill AH, Jr., Schmelz EM, Dillehay DL, Spiegel S, Shayman JA, Schroeder JJ, et al. Sphingolipids--the enigmatic lipid class: biochemistry, physiology, and pathophysiology. *Toxicol Appl Pharmacol.* 1997;142(1):208-25.
8. Hanada K, Kumagai K, Yasuda S, Miura Y, Kawano M, Fukasawa M, et al. Molecular machinery for non-vesicular trafficking of ceramide. *Nature.* 2003;426(6968):803-9.
9. Bienias K, Fiedorowicz A, Sadowska A, Prokopiuk S, and Car H. Regulation of sphingomyelin metabolism. *Pharmacol Rep.* 2016;68(3):570-81.
10. Adada M, Luberto C, and Canals D. Inhibitors of the sphingomyelin cycle: Sphingomyelin synthases and sphingomyelinases. *Chem Phys Lipids.* 2016;197:45-59.
11. Sabourdy F, Astudillo L, Colacios C, Dubot P, Mrad M, Segui B, et al. Monogenic neurological disorders of sphingolipid metabolism. *Biochim Biophys Acta.* 2015;1851(8):1040-51.
12. Astudillo L, Sabourdy F, Therville N, Bode H, Segui B, Andrieu-Abadie N, et al. Human genetic disorders of sphingolipid biosynthesis. *J Inherit Metab Dis.* 2015;38(1):65-76.
13. Mosbech MB, Olsen AS, Neess D, Ben-David O, Klitten LL, Larsen J, et al. Reduced ceramide synthase 2 activity causes progressive myoclonic epilepsy. *Ann Clin Transl Neurol.* 2014;1(2):88-98.
14. Vanni N, Fruscione F, Ferlazzo E, Striano P, Robbiano A, Traverso M, et al. Impairment of ceramide synthesis causes a novel progressive myoclonus epilepsy. *Ann Neurol.* 2014;76(2):206-12.
15. Ferlazzo E, Striano P, Italiano D, Calarese T, Gasparini S, Vanni N, et al. Autosomal recessive progressive myoclonus epilepsy due to impaired ceramide synthesis. *Epileptic Disord.* 2016;18(S2):120-7.
16. Fragaki K, Ait-El-Mkadem S, Chaussenot A, Gire C, Mengual R, Bonesso L, et al. Refractory epilepsy and mitochondrial dysfunction due to GM3 synthase deficiency. *Eur J Hum Genet.* 2013;21(5):528-34.
17. Simpson MA, Cross H, Proukakis C, Priestman DA, Neville DC, Reinkensmeier G, et al. Infantile-onset symptomatic epilepsy syndrome caused by a homozygous loss-of-function mutation of GM3 synthase. *Nat Genet.* 2004;36(11):1225-9.
18. Boukhris A, Schule R, Loureiro JL, Lourenco CM, Mundwiller E, Gonzalez MA, et al. Alteration of ganglioside biosynthesis responsible for complex hereditary spastic paraparesis. *Am J Hum Genet.* 2013;93(1):118-23.

19. Janecke AR, Xu R, Steichen-Gersdorf E, Waldegger S, Entenmann A, Giner T, et al. Deficiency of the sphingosine-1-phosphate lyase SGPL1 is associated with congenital nephrotic syndrome and congenital adrenal calcifications. *Hum Mutat*. 2017;38(4):365-72.
20. Lovric S, Goncalves S, Gee HY, Oskouian B, Srinivas H, Choi WI, et al. Mutations in sphingosine-1-phosphate lyase cause nephrosis with ichthyosis and adrenal insufficiency. *J Clin Invest*. 2017;127(3):912-28.
21. Prasad R, Hadjidemetriou I, Maharaj A, Meimarisou E, Buonocore F, Saleem M, et al. Sphingosine-1-phosphate lyase mutations cause primary adrenal insufficiency and steroid-resistant nephrotic syndrome. *J Clin Invest*. 2017;127(3):942-53.
22. Atkinson D, Nikodinovic Glumac J, Asselbergh B, Ermanoska B, Blocquel D, Steiner R, et al. Sphingosine 1-phosphate lyase deficiency causes Charcot-Marie-Tooth neuropathy. *Neurology*. 2017;88(6):533-42.
23. Steiner R, Saied EM, Othman A, Arenz C, Maccarone AT, Poad BL, et al. Elucidating the chemical structure of native 1-deoxysphingosine. *J Lipid Res*. 2016;57(7):1194-203.
24. Vesper H, Schmelz EM, Nikolova-Karakashian MN, Dillehay DL, Lynch DV, and Merrill AH. Sphingolipids in food and the emerging importance of sphingolipids to nutrition. *Journal of Nutrition*. 1999;129(7):1239-50.
25. Causerset C, Geeraert L, Van der Hoeven G, Mannaerts GP, and Van Veldhoven PP. Further characterization of rat dihydroceramide desaturase: tissue distribution, subcellular localization, and substrate specificity. *Lipids*. 2000;35(10):1117-25.
26. Cadena DL, Kurten RC, and Gill GN. The product of the MLD gene is a member of the membrane fatty acid desaturase family: overexpression of MLD inhibits EGF receptor biosynthesis. *Biochemistry*. 1997;36(23):6960-7.
27. Sperling P, Zahringer U, and Heinz E. A sphingolipid desaturase from higher plants. Identification of a new cytochrome b5 fusion protein. *J Biol Chem*. 1998;273(44):28590-6.
28. Holland WL, Brozinick JT, Wang LP, Hawkins ED, Sargent KM, Liu Y, et al. Inhibition of ceramide synthesis ameliorates glucocorticoid-, saturated-fat-, and obesity-induced insulin resistance. *Cell Metab*. 2007;5(3):167-79.
29. Mizutani Y, Kihara A, and Igashira Y. Identification of the human sphingolipid C4-hydroxylase, hDES2, and its up-regulation during keratinocyte differentiation. *FEBS Lett*. 2004;563(1-3):93-7.
30. Holland WL, and Summers SA. Strong Heart, Low Ceramides. *Diabetes*. 2018;67(8):1457-60.
31. Summers SA. Could Ceramides Become the New Cholesterol? *Cell Metab*. 2018;27(2):276-80.
32. Vieira CR, Munoz-Olaza JM, Sot J, Jimenez-Baranda S, Izquierdo-Useros N, Abad JL, et al. Dihydrophingomyelin impairs HIV-1 infection by rigidifying liquid-ordered membrane domains. *Chem Biol*. 2010;17(7):766-75.
33. Aggarwal S, Yurlova L, and Simons M. Central nervous system myelin: structure, synthesis and assembly. *Trends Cell Biol*. 2011;21(10):585-93.
34. Nolte KW, Hans VJ, Schattenfroh C, Weis J, and Schroder JM. Perineurial cells filled with collagen in 'atypical' Cogan's syndrome. *Acta Neuropathol*. 2008;115(5):589-96.
35. Guo Y, Ding X, Shen Y, Lyon GJ, and Wang K. SeqMule: automated pipeline for analysis of human exome/genome sequencing data. *Sci Rep*. 2015;5:14283.

36. Li MX, Kwan JS, Bao SY, Yang W, Ho SL, Song YQ, et al. Predicting mendelian disease-causing non-synonymous single nucleotide variants in exome sequencing studies. *PLoS Genet.* 2013;9(1):e1003143.
37. Esmaeili M, Jennek S, Ludwig S, Klitzsch A, Kraft F, Melle C, et al. The tumor suppressor ING1b is a novel corepressor for the androgen receptor and induces cellular senescence in prostate cancer cells. *J Mol Cell Biol.* 2016;8(3):207-20.
38. Pellegrino RM, Di Veroli A, Valeri A, Goracci L, and Cruciani G. LC/MS lipid profiling from human serum: a new method for global lipid extraction. *Anal Bioanal Chem.* 2014;406(30):7937-48.
39. Narvaez-Rivas M, and Zhang Q. Comprehensive untargeted lipidomic analysis using core-shell C30 particle column and high field orbitrap mass spectrometer. *J Chromatogr A.* 2016;1440:123-34.
40. Alecu I, Othman A, Penno A, Saied EM, Arenz C, von Eckardstein A, et al. Cytotoxic 1-deoxysphingolipids are metabolized by a cytochrome P450-dependent pathway. *J Lipid Res.* 2017;58(1):60-71.

Figure and Table legends

Figure 1

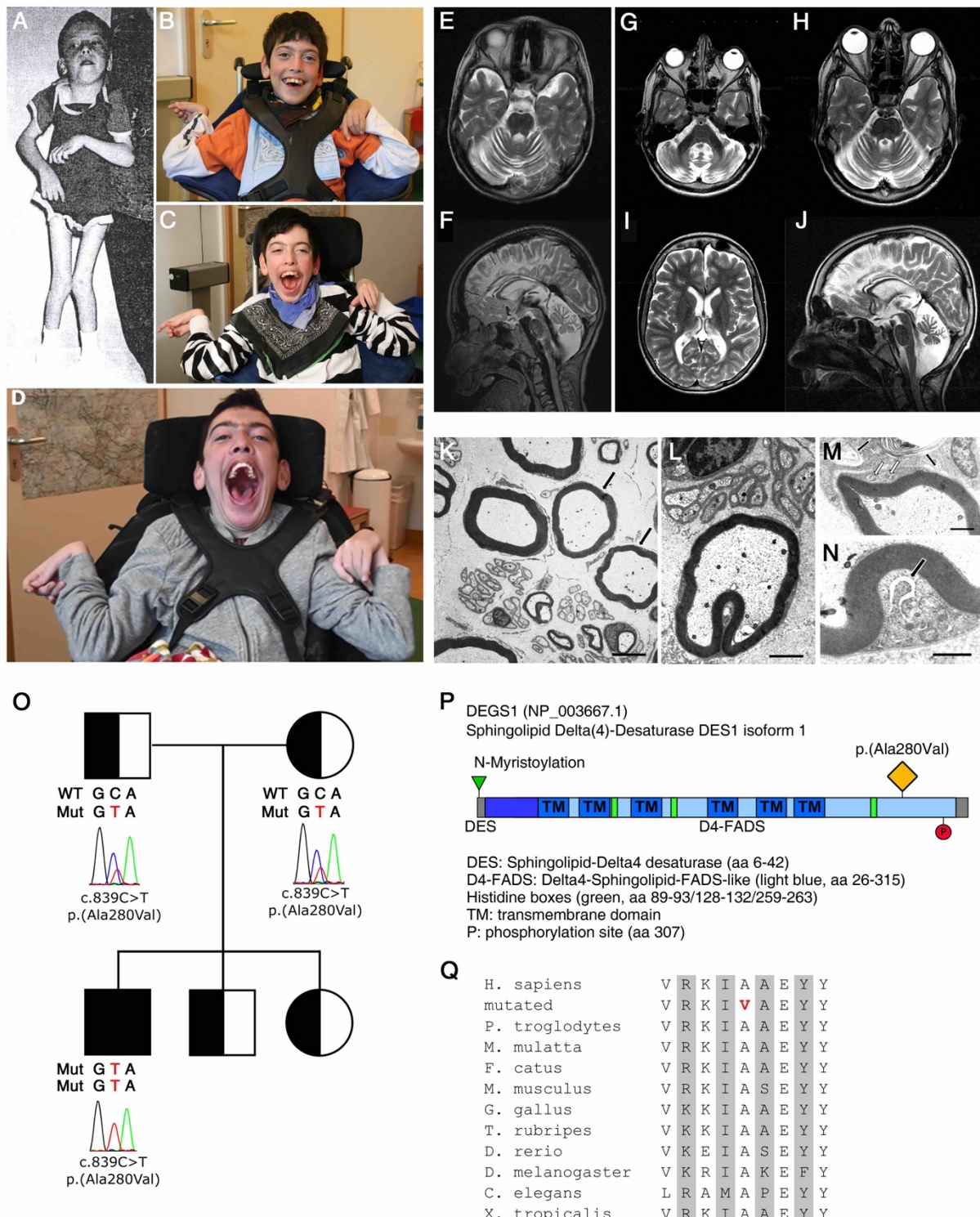


Figure 1: Clinical phenotype and genetics of the DEGS1 disorder. Clinical phenotype with progression of spasticity, notably in arms and hands. Patient at the age of 6 years (A), 13 years (B), 15 years (C) and at last follow up with 22 years (D). T2-weighted magnetic resonance imaging of the brain, axial (E; G-I) and sagittal (F; J), at 11 years of age (E-F) and 16 years (G-J).

J). Severe and slowly progressive cerebellar atrophy with fiber degeneration of the middle cerebellar peduncles. The patient shows mild cortical atrophy and thin white matter especially in the posterior brain regions. In summary, MRI findings are in line with a progressive global neurodegenerative process. **(K-N)** Electron micrographs of the sural nerve biopsy performed at the age of two years reveals nerve fibers with disproportionately thin myelin sheaths **(K)**, arrows). Scale bar = 3 μ m. **(L)** Occasional, moderate myelin folding. Scale bar = 1.8 μ m. **(M)** Small autophagic vacuoles in the cytoplasm of the Schwann cell of a myelinated nerve fiber (white arrows); black arrows: large autophagic vacuoles containing membranous debris in an adjacent cell which is covered by a basal lamina and may therefore be either a Schwann cell or a macrophage that has invaded a Schwann cell basal lamina sheath. Scale bar = 0.75 μ m. **(N)** Widening of the endoplasmic reticulum (arrow) of a Schwann cell. Scale bar = 0.5 μ m. **(O)** The pedigree of the family shows the segregation of the *DEGS1* variant (NM_003676.3:c.839C>T, p.(Ala280Val), Chr1(hg19):g.224380047C>T) in the family. Sanger traces of the affected codon are shown in the index patient and his parents. **(P)** Domain architecture of the human *DEGS1* protein. Position of the mutation indicated in orange. **(Q)** Species alignment of the amino acid residues in proximity of the *DEGS1* mutation. Mutation highlighted in red.

Figure 2

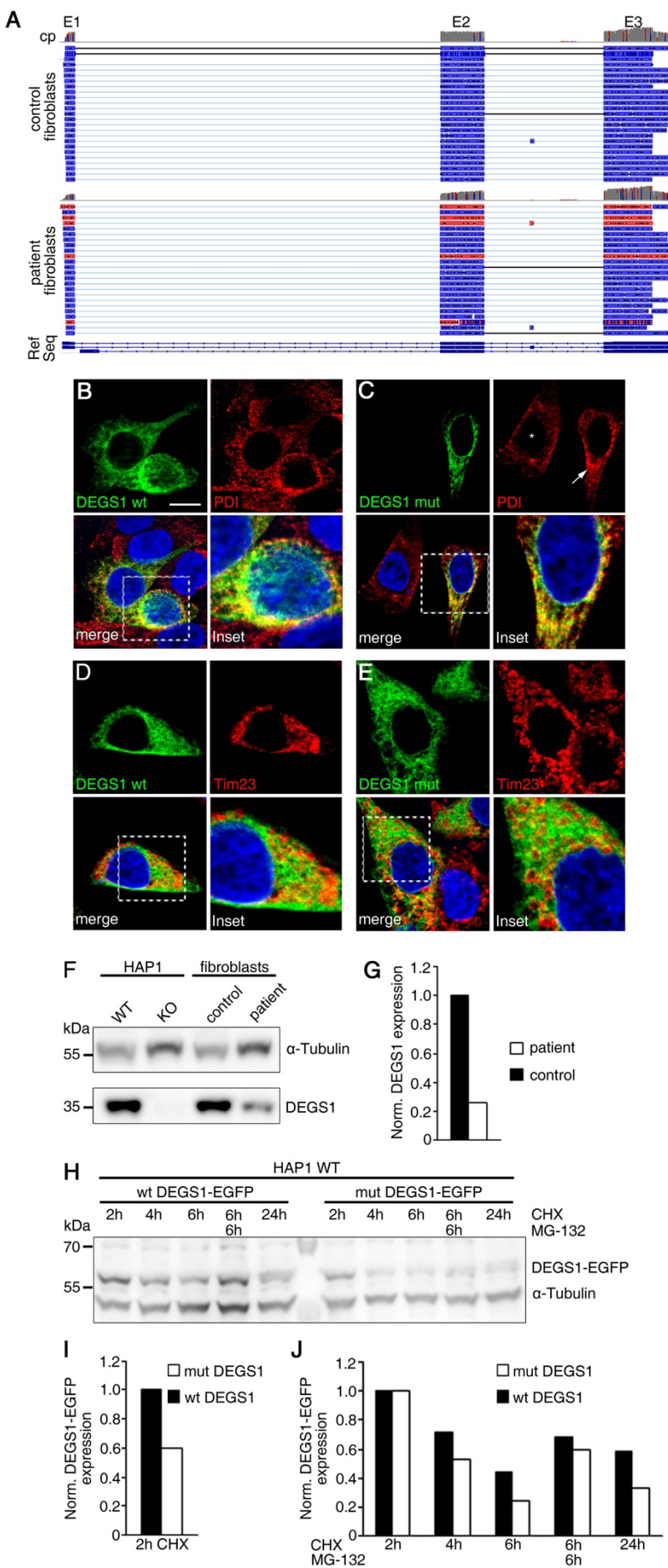


Figure 2: Characterization of mutant DEGS1 proteins. The DEGS1 mutant decreases protein stability. **(A)** IGV plots of direct cDNA nanopore sequencing results. The upper part of each plot shows the coverage plot (cp, grey) and the lower part the single reads. **(B-E)** Cellular distribution of DEGS1 wt and the DEGS1 mutant (p.Ala280Val). EGFP-tagged **(B)** wt and **(C)** mutant DEGS1 colocalize with the endoplasmic reticulum-marker protein disulfide-isomerase (PDI). The reticular staining pattern of PDI in untransfected cells (asterisk in C) seems not disturbed in mut DEGS1 overexpressing cells (arrow in C). **(D, E)** Only minor overlap of immunofluorescence signals is observed for wt and mutant EGFP-tagged DEGS1 overexpressing cells with the mitochondrion inner membrane marker Tim23. Scale bars: 10 μ m. Blow-ups 5 μ m scale. **(F, G)** DEGS1 expression was analyzed by Western Blot in HAP1 WT and HAP1 DEGS1^{-/-} cells or fibroblasts from a healthy control and the index patient. **(G)** Reduced DEGS1 protein levels in patient fibroblasts, quantified from blot in F (normalized to α -tubulin and the control sample). **(H)** DEGS1-EGFP expression in HAP1 WT cells transfected with pEF1 α -wt DEGS1-EGFP/mut DEGS1-EGFP after treatment with cycloheximide (CHX) and MG-132 for the indicated times. **(I,J)** Quantification of wt and mut DEGS1-EGFP protein amounts from (H) normalized to α -tubulin and DEGS1-EGFP (I) or wt DEGS1-EGFP and mut DEGS1-EGFP (J). kDa - kilo Dalton.

Figure 3

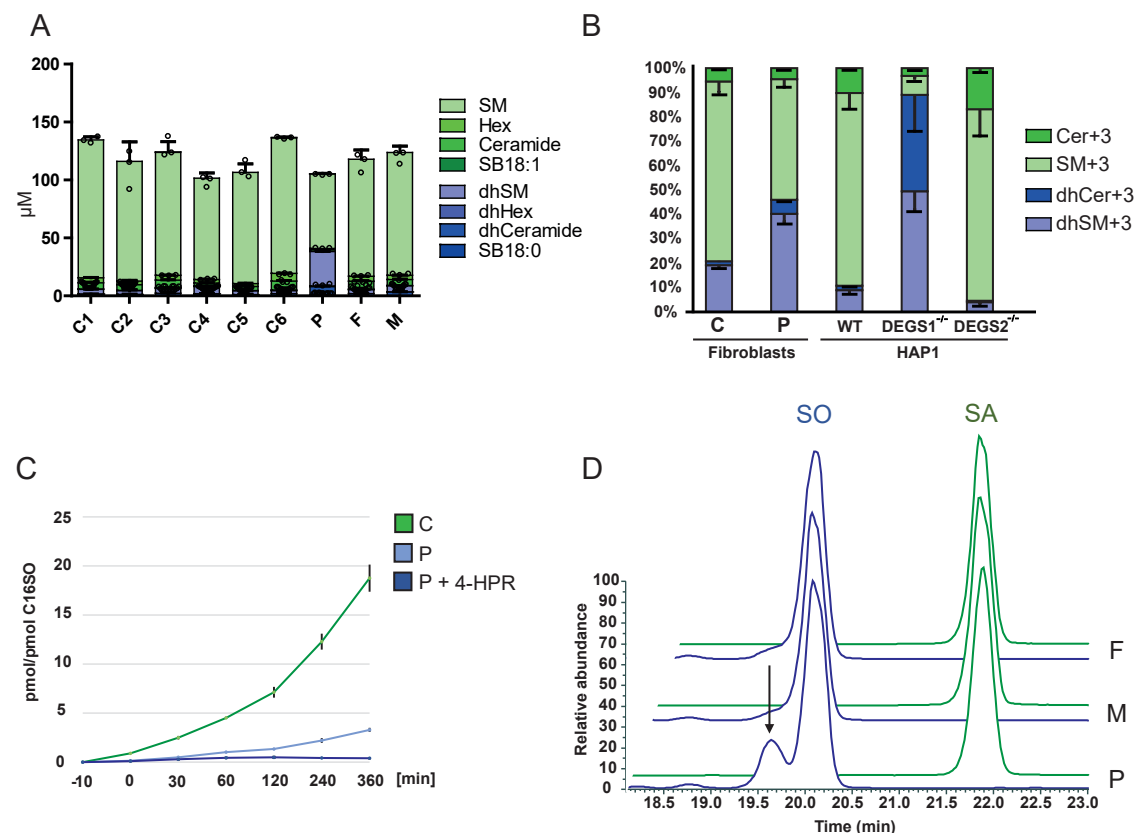


Figure 3: Lipidomics analysis of mutant DEGS1. (A) Lipidomics analysis showed a significant elevation of dhSL species (dhCer, dhSM and dhHexCer) in patient plasma (P) compared to parents (F,M) or unrelated controls (C1-6). N=3; Error bars indicate SD. (B) Cultured patient-derived fibroblast showed an increase in de novo synthesized dhSL (dhCer+3 and dhSM+3) compared to cells from unrelated controls. Increased dhSL levels were also seen in DEGS1^{-/-} HAP1 cells where the dhSL species reached up to 90% of the total SLs. In contrast, wt cells had less than 15% dhSL species. Slightly decreased dhSL levels were observed in DEGS2^{-/-} cells. N=3. Error bars indicate SD. (C) Kinetic of the DEGS1 reaction in control and patient fibroblasts. Cells were supplemented with 2 μ M d7-SA (arrow) and the increase in total SO+7 was followed over time. In patient-derived fibroblasts, DEGS1 activity was fivefold lower compared to controls. This residual activity was fully inhibited in presence of the DEGS1 inhibitor 4-HPR (2 μ M). N=3; Error bars indicate SD (D) The sphingoid base profile after hydrolysis revealed an isomeric SO metabolite (arrow) with an about 30 seconds shorter retention time. The metabolite could be detected in patient plasma but not in plasma of the parents or unrelated controls. No isomeric peak was seen for SA (green).

Figure 4

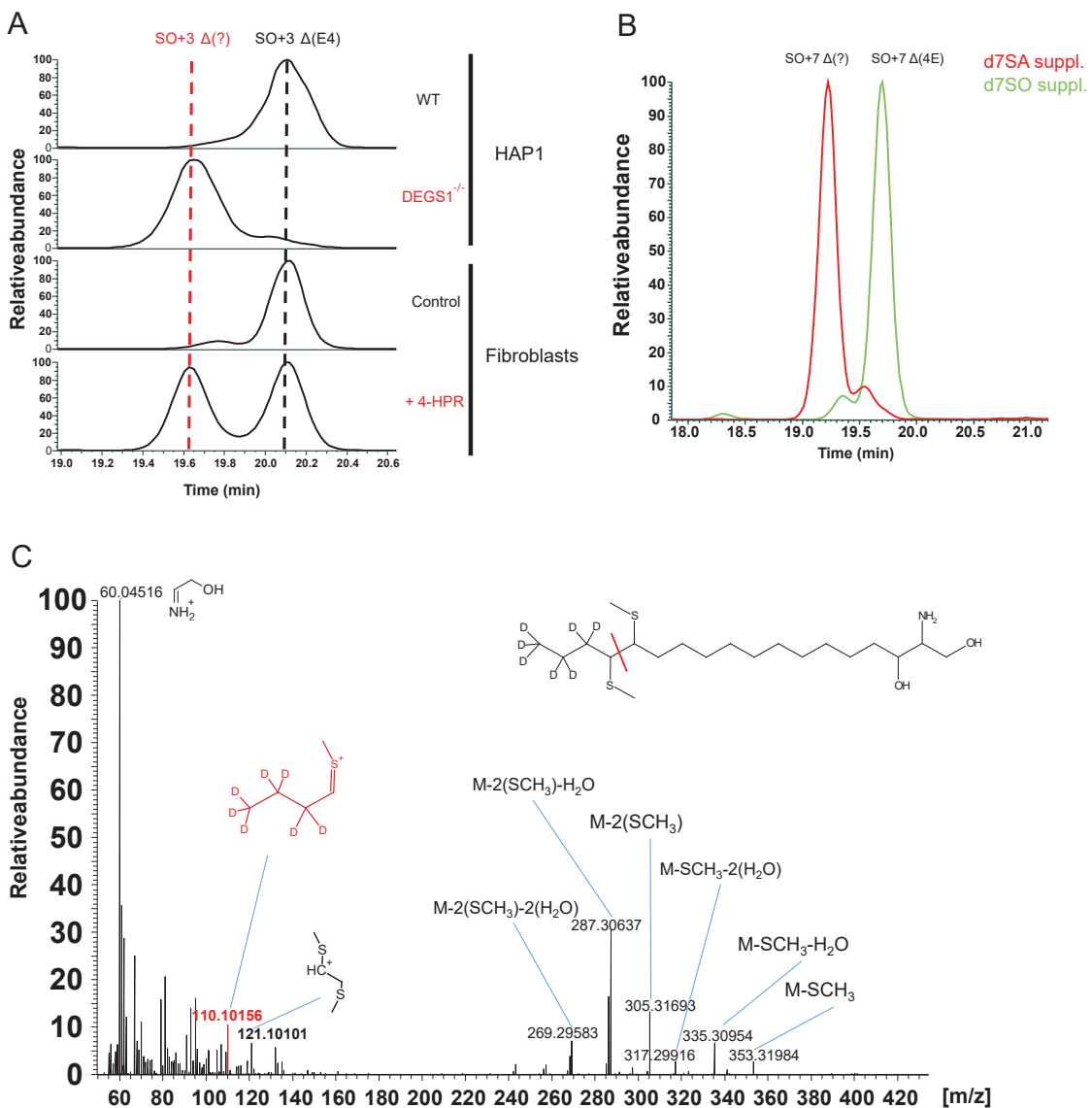


Figure 4: Characterization of a novel sphingoid base in the DEGS1 disorder. (A) HAP1 wt / DEGS1^{-/-} cells were cultured in presence of isotope labelled d4-serine. Whereas HAP1 wt cells only formed canonical SO+3, DEGS1^{-/-} cells exclusively formed the new SO+3 isomer. Similarly, wildtype fibroblasts primarily formed canonical SO+3 when cultured in the presence of d4-serine while the new SO+3 isomer was formed when DEGS1 activity was inhibited with 4-HPR. (B) DEGS1^{-/-} cells were supplemented with isotope labelled d7SA (1uM) or d7SO (1uM) for 24h. The isomeric SO was formed only in d7SA, but not in d7SO supplemented cells (C) Structural analysis of the +7 labelled isomeric SO (SOΔ(?)) after chemical derivatization with dimethyl disulfide. A specific collision fragment with a m/z 110.10156 reflecting the isotope labelled four carbon tail of SO+7 proved that the double bond of the isomeric SO isomer is in Δ14 position.

DEGS1 (NM_003676.3)	c.839C>T; p.(Val280Ile)
Chromosomal position (hg19)	chr1:224380047C>T
Origin	Turkey (consanguineous parents)
Gender	Male
Age at onset	6 months
Age at last follow-up	21 years (y)
Clinical diagnosis	Multisystem disorder with progressive tetraspasticity, epilepsy, mental retardation, microcephaly
Clinical phenotype at last follow-up	Intellectual disability, non-ambulatory, severe spasticity, non-verbal, friendly
Body Weight	Normal at birth, dystrophy since the age of 3 y; at last follow-up 43 kg (-3.7 SD); percutan gastrostomy since age 18 y
Body Length	Normal at birth, mild short stature since the age of 4.5 y; at last follow-up 160 cm (-2.5 SD)
Head circumference	Normal in the first year than progressive microcephaly; at last follow-up 53 cm (-2.5 SD)
Epilepsy	Onset 5 years, grand mal epilepsy; under therapy with valproate and carbamazepin, since age 11 y no seizures
Brain MRI	Cerebellar atrophy, mild global atrophy thin white matter especially in the posterior brain regions
Visual evoked potentials	Pathological latency
Acustic evoked potentials	Pathological latency
BERA	Pathologcial interpeak latency / auditory threshold 85 db
Electroneurography	Mild demyelinating neuropathy with decreased motoric nerve conduction velocities (mNCV): mNCV N. medianus 30.0 m/s age 2 y; 28.7 m/s age 12 y mNCV N. tibialis 38.0 m/s age 2 y; 39.2 m/s age 12 y
Nerve biopsy	Peripheral hypomyelination
Muscular biopsy	Neurogenic muscular atrophy
Scoliosis	Scoliosis surgery at age 18 y
Neurogenic bladder disorder	Present

Table 1: Clinical findings in the affected individual.